A coupling of linear potential flow model based on Poincaré's velocity representation and viscous flow model based on SWENSE

Young-Myung Choi[1], Benjamin Bouscasse[1], Lionel Gentaz[1], Pierre Ferrant[1], and Šime Malenica[2]

[1] *LHEEA, Ecole Centrale de Nantes, Nantes, France CNRS UMR 6598*

[2] *Bureau Veritas, Paris, France*

Introduction

The present study aims to couple a nonlinear viscous flow model based on the Spectral Wave Explicit Navier-Stokes Equation (SWENSE) method and a linear potential flow model which is based on Poincaré's velocity representation. A circular cylindrical matching surface is introduced for the potential flow model to update the far-field domain with efficiency and stability. A relaxation scheme, which blends the solution of viscous flow with a target solution, is used to update the far-field boundary conditions of viscous flow solver.

Assumptions and coupling strategy

The hypothesis that the total solution (functional quantities) can be decomposed into the incident and complementary parts is adopted. The nonlinear incident solution is already known from potential flow theory in a whole fluid domain. The computational domain of potential and viscous flow models are divided for complementary flow. A viscous flow model based on the SWENSE method is used to compute the complementary flow near to the body [2]. A linear potential flow model based on Poincaré's velocity representation is adopted to compute the complementary flow in the far-field.

Figure 1 illustrates the coupling strategy. Fluid velocity and wave elevations are coupled on the matching surface for potential flow and in the relaxation zone for viscous flow. The matching surface is located inside the computational domain of the viscous flow model. The complementary fluid velocity and wave elevation, obtained from the viscous flow model on the matching surface, are used as boundary conditions for the potential flow model. The rotational velocity components are assumed to be zero from the matching surface to infinity. By using the linear potential flow model, the complementary fluid velocity and wave elevation are reconstructed in the far-field. In the relaxation zone, being located in the region of far-field, reconstructed complementary flow velocity and wave elevation from the linear potential flow model are imposed as boundary conditions for viscous flow.

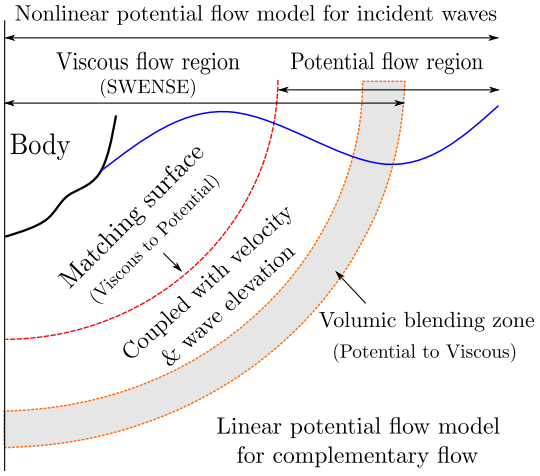

Figure 1: Coupling strategy

Potential and viscous flow models

Linear potential flow model based on Poincaré's velocity representation

The Poincaré's velocity representation is an alternative expression of Boundary Integral Equation (BIE) for the fluid velocity at the field point. This representation was introduced by [7] for steady and time-harmonic problems with the existence of free surface. Recently, [1] extended the representation for an unsteady problem without forward speed. The final fluid velocity representation at any field point is expressed explicitly with fluid velocity on the matching surface and wave elevation along its waterline. A vertical circular cylindrical matching surface is introduced to remedy a singular behavior, which was reported in [1]. The Green's function and complementary parts are expanded with the Fourier and Fourier-Laguerre series, as similar to [5]. After manipulation, the final velocity representation at any field point is given explicitly as:

$$\begin{bmatrix} u_C^x \\ u_C^y \\ u_C^z \end{bmatrix}(r,\theta,z) = \frac{1}{4\pi}\sum_{n=-N}^{N}\sum_{p=0}^{M}\begin{bmatrix} \mathcal{U}_{pn}^x(r) \\ \mathcal{U}_{pn}^y(r) \\ \mathcal{U}_{pn}^z(r) \end{bmatrix} e^{in\theta}\mathcal{L}_p(-sz) \qquad \text{with} \qquad \begin{aligned} \mathcal{U}_{pn}^x(r) &= \mathcal{U}_{pn}^{Rx} + \mathcal{U}_{pn}^{Rx*} + \mathcal{U}_{pn}^{Hx} + \mathcal{U}_{pn}^{Fx} \\ \mathcal{U}_{pn}^y(r) &= \mathcal{U}_{pn}^{Ry} + \mathcal{U}_{pn}^{Ry*} + \mathcal{U}_{pn}^{Hy} + \mathcal{U}_{pn}^{Fy} \\ \mathcal{U}_{pn}^z(r) &= \mathcal{U}_{pn}^{Rz} + \mathcal{U}_{pn}^{Rz*} + \mathcal{U}_{pn}^{Hz} + \mathcal{U}_{pn}^{Fz} \end{aligned} \tag{1}$$

where u_C is the fluid velocity at the field point $\mathbf{x} = (r, \theta, z)$. The superscripts ^{x,y,z} denote directional components, respectively. $\mathcal{U}_{pn}(r)$ is the Fourier-Laguerre coefficient. $\mathcal{L}_p(-sz) = e^{\frac{s}{2}z} L_m(-sz)$ is Laguerre function with Laguerre polynomials $L_m(-sz)$. s is an approximation parameter. $\mathcal{U}^R_{pn}$,$\mathcal{U}^{R*}_{pn}$,$\mathcal{U}^H_{pn}$ and $\mathcal{U}^F_{pn}$ are contributions of source, image source, harmonic term and free surface, respectively. For example, x-directional components are given as:

$$\mathcal{U}^{Rx}_{pn} + \mathcal{U}^{Rx*}_{pn} = \frac{1}{2}\sum_{n=-N}^{N}\sum_{m=0}^{M}[\left(\mathcal{C}^n_{mn+1} + \mathcal{C}^n_{mn-1} + \mathrm{i}\mathcal{W}^z_{mn+1} - \mathrm{i}\mathcal{W}^z_{mn-1}\right)\left(\mathcal{S}^R_{a,n,mp} + \mathcal{S}^{R*}_{a,n,mp}\right) - 2\mathcal{W}^y_{mn}(\mathcal{S}^R_{\zeta,n,mp} + \mathcal{S}^{R*}_{\zeta,n,mp}) + \left(\mathcal{W}^z_{mn+1} + \mathcal{W}^z_{mn-1} - \mathrm{i}\mathcal{C}^n_{mn+1} + \mathrm{i}\mathcal{C}^n_{mn-1}\right)\left(\mathcal{S}^R_{\theta',n,mp} + \mathcal{S}^{R*}_{\theta',n,mp}\right)] \tag{2}$$

$$\mathcal{U}^{Hx}_{pn} = -\frac{1}{2}\sum_{n=-N}^{N}\sum_{m=0}^{M}\int_{t_0}^{t}[\left(\mathcal{C}^n_{mn+1} + \mathcal{C}^n_{mn-1} + \mathrm{i}\mathcal{W}^z_{mn+1} - \mathrm{i}\mathcal{W}^z_{mn-1}\right)\mathcal{S}^H_{a,n,mp} - 2\mathcal{W}^y_{mn}\mathcal{S}^H_{\zeta,n,mp} + \left(\mathcal{W}^z_{mn+1} + \mathcal{W}^z_{mn-1} - \mathrm{i}\mathcal{C}^n_{mn+1} + \mathrm{i}\mathcal{C}^n_{mn-1}\right)\mathcal{S}^H_{\theta',n,mp}]d\tau \tag{3}$$

$$\mathcal{U}^{Fx}_{pn} = -\frac{1}{2}\sum_{n=-N}^{N}\int_{t_0}^{t}(\mathcal{E}_{n+1} + \mathcal{E}_{n-1})\mathcal{F}^F_{\zeta,n,p} \tag{4}$$

where $\mathcal{C}^n_{mn}$, $\mathcal{W}_{mn}$ and $\mathcal{E}_n$ are Fourier-Laguerre and Fourier coefficients defined on the matching surface and its waterline as:

$$\begin{bmatrix}\mathcal{C}^{\mathbf{n}}_{mn}\\ \mathcal{W}_{mn}\end{bmatrix} = \frac{s}{2\pi}\int_0^{2\pi}\int_{-\infty}^{0}\begin{bmatrix}u^{\mathbf{n}}_C\\ w_C\end{bmatrix}_{r=a}\mathcal{L}_m\left(-s\zeta\right)e^{-in\theta'}d\zeta d\theta' \qquad \text{and} \qquad \mathcal{E}_n = \frac{1}{2\pi}\int_0^{2\pi}\left[g\Xi_C\right]_{r=a}e^{-in\theta'}d\theta' \tag{5}$$

where $u^{\mathbf{n}}_C$, w_C and Ξ_C are normal and tangential fluid velocity on the matching surface and complementary wave elevation along the waterline which are obtained from the viscous flow solver, respectively. $\mathcal{S}_{n,mp}$ and $\mathcal{F}^F_{n,p}$ are elementary functions, superscripts ^{R,R*,H,F} denote components of Green's function and subscripts $_{a,\theta',\zeta}$ correspond to the directional derivatives, respectively. General forms of elementary function are defined as:

$$\mathcal{S}_{n,mp}(r,a,t-\tau) = 2\pi as\int_{-\infty}^{0}\int_{-\infty}^{0}\mathcal{L}_m(-s\zeta)\mathcal{L}_p(-sz)G_n(r,z,a,\zeta,t-\tau)d\zeta dz \tag{6}$$

$$\mathcal{F}_{n,p}(r,a,t-\tau) = 2\pi as\int_{-\infty}^{0}\mathcal{L}_p(-sz)G_n(r,z,a,\zeta=0,t-\tau)dz \tag{7}$$

where $G_n(r,z,a,\zeta,t-\tau)$ is the n-th Fourier mode of Green's function. The complementary wave elevation in the far-field is updated by using the linear kinematic free surface boundary condition.
The benchmark test is conducted for a linear diffraction problem of a vertical circular cylinder in regular waves. Complementary fluid velocity and wave elevation on the matching surface from analytic solutions are used to reconstruct the fluid velocity and wave elevation at the field point by using the Poincaré's velocity representation. Reconstructed wave field and fluid velocity for the diffraction of a vertical circular cylinder are shown in Figure 2.

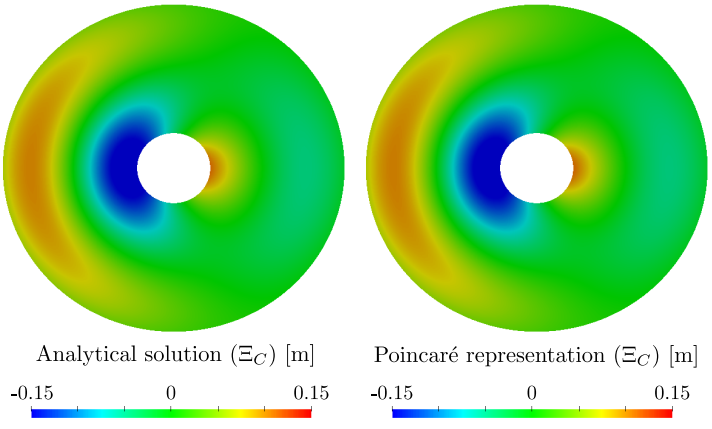

(a) Wave elevation field

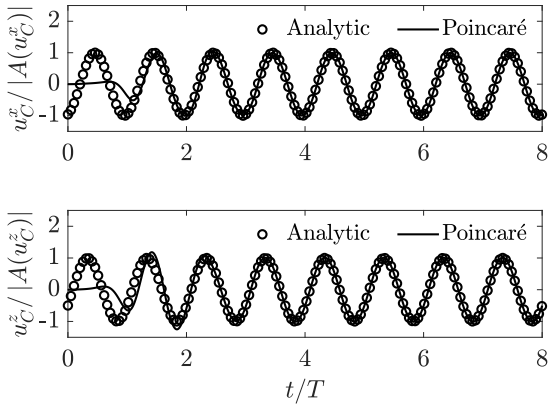

(b) Fluid velocity on the mean free surface

Figure 2: Reconstructed wave elevation and fluid velocity by using the Poincaré's velocity representation.

Multiphase SWENSE with Level-set function

The SWENSE method was introduced for a single-phase flow by [2] and for a multiphase flow by [4, 9]. In multiphase flow, functional quantities such as velocity, pressure and Level-set (LS) function can be decomposed into the incident and complementary parts by combining ideas of [4, 9] as follows:

$$\mathbf{u} = \mathbf{u}_I + \mathbf{u}_C, \qquad p = p_I + p_C, \qquad \psi = \psi_I + \psi_C \tag{8}$$

where $\mathbf{u}$, p and ψ are fluid velocity, pressure and LS function, respectively. The subscripts $_I$ and $_C$ represent incident and complementary parts, respectively. Substituting above relation into the Navier-Stokes (NS) equations and LS transport equation gives governing equations for complementary parts as:

$$\nabla \cdot \mathbf{u}_C = 0 \tag{9}$$

$$\frac{\partial \mathbf{u}_C}{\partial t} + \nabla \cdot (\mathbf{u}\mathbf{u}_C) + \mathbf{u}_C \cdot \nabla \mathbf{u}_I = -\frac{1}{\rho}\nabla p_C - \frac{p_I}{\rho_w}\frac{\nabla \rho}{\rho} + \nabla \cdot \left(\nu \left(\nabla \mathbf{u}_C + \nabla \mathbf{u}_C^T\right)\right) \tag{10}$$

$$\frac{\partial \psi_C}{\partial t} + \nabla \cdot (\mathbf{u}\psi_C) = -\frac{\partial \psi_I}{\partial t} - \nabla \cdot (\mathbf{u}\psi_I) \tag{11}$$

where ρ and ρ_w are mixture and water density, respectively [4]. In the framework of OpenFOAM, governing equations are discretized on a collocated Finite Volume (FV) with second-order accuracy.
The far-field boundary conditions for the viscous flow model are imposed by using a relaxation scheme to generate/absorb complementary waves as:

$$\psi_C = (1-w)\psi_C + w\psi_C^{\text{Poincaré}} \qquad \text{and} \qquad \mathbf{u}_C = (1-w)\mathbf{u}_C + w\mathbf{u}_C^{\text{Poincaré}} \tag{12}$$

where $w = [0, 1]$ is a weight function varying from 0 to 1 in the relaxation zone. The superscript $^{\text{Poincaré}}$ denotes the functional quantity obtained from the linear potential flow model based on Poincaré's velocity representation.

Benchmark test on the coupling

A benchmark test on the coupling is conducted for the diffraction problem by a vertical circular cylinder in regular waves. The computation configuration is shown in Figure 3. The grey colored zone denotes the computational domain of viscous flow solver and the relaxation zone is defined from a red dashed circle to the end of the grey zone. The vertical circular cylindrical matching surface is defined with red-colored dots. Red-colored dots represent Gauss points where complementary fluid velocity and wave elevation are obtained from the viscous flow solver. The far-field solution, reconstructed from the Poincaré's velocity representation, is used as a target solution to update far-field boundary conditions of the viscous flow solver.

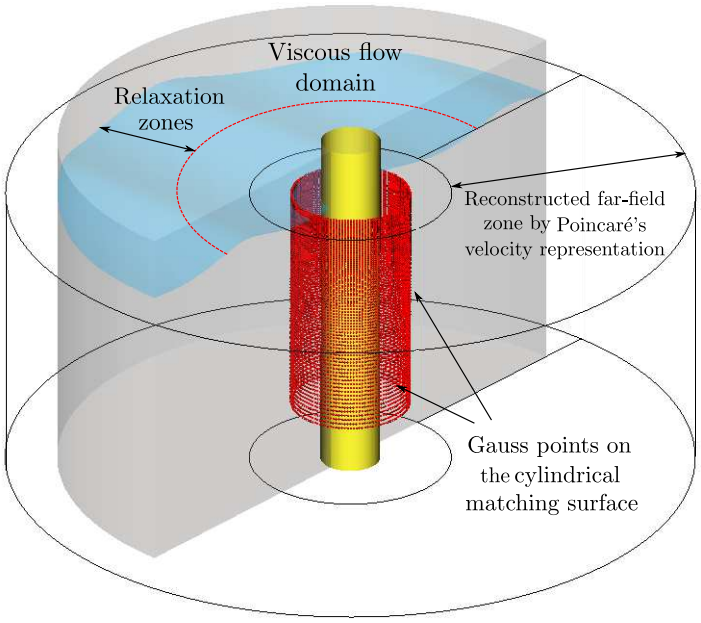

Figure 3: Computational domain of viscous and potential flow models for benchmark test case on a vertical circular cylinder in regular waves.

Computed complementary wave elevation fields are compared in Figure 4 with respect to the application of coupling, where k_0 is the wavenumber and $a_{cylinder}$ is a radius of the cylinder. When the coupling is considered, the matching surface is located at $2a_{cylinder}$. In Figure 4, complementary waves are propagating up to the far-field and smooth transition across the relaxation zone are observed when the coupling is applied.
The harmonic and mean components of horizontal force acting on the cylinder are compared in Figure 5 with the analytical solution of potential theory [6], results of Higher-Order Boundary Element Method (HOBEM) [3] and results by a viscous flow solver solving the NS equations in a large computational domain [8].

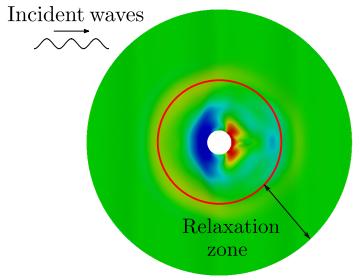

(a) without coupling, $t = 12T$

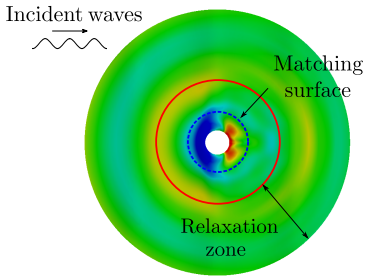

(b) with coupling, $t = 12T$

Figure 4: Complementary wave elevation fields with respect to application of coupling for the case of $k_0 a_{cylinder} = 1.0$.

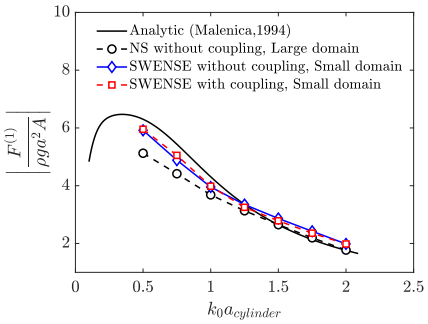

(a) First harmonic, $F^{(1)}$

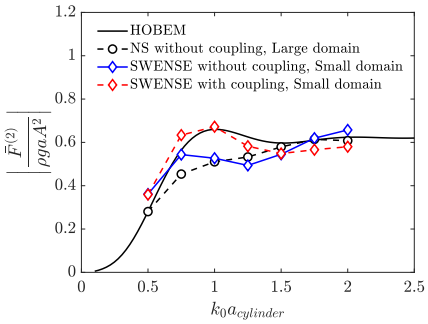

(b) Mean drift force, $\bar{F}^{(2)}$

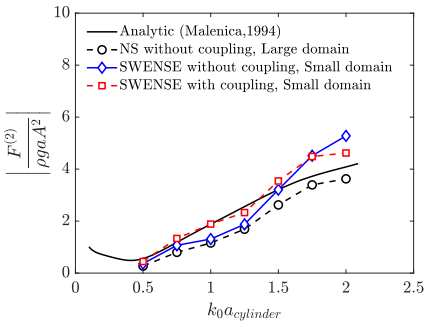

(c) Second harmonic, $F^{(2)}$

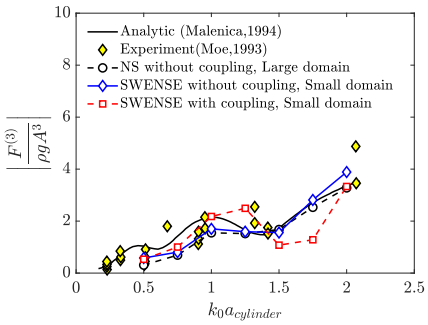

(d) Third harmonic, $F^{(3)}$

Figure 5: Horizontal force harmonics and mean drift forces with respect to the two-way coupling for different viscous flow models.

When the coupling is applied, the first and second harmonics are slightly improved compared to results without considering coupling. The mean drift forces have enhanced results when the coupling is adopted. However, no improvements are observed for the third harmonics because poor results are obtained on the magnitude of forces for all simulations. The extra computational time for coupling is measured less than a couple of seconds (in the present study: $\leq 2s$) for each time step which is relatively smaller than the computational time needed for viscous flow solver (usually in the range of $O(10s)$ per time step).

To conclude, the computational domain can be reduced when the coupling between potential and viscous flow is adopted. Especially, the horizontal mean drift forces acting on the structure are enhanced. The computation cost slightly increases, but it is negligible compared to the computational cost needed to solve the viscous flow model. However, the algorithm complexity is increased and it is still to be understood how efficient for practical cases.

Acknowledgement

This work has been performed in the framework of the Chaire Hydrodynamique et Structure Marines CENTRALE NANTES - BUREAU VERITAS. The support a National Research Foundation of Korea (NRF) grant funded by the Korean Government (MSIP) through GCRC-SOP (Grant No. 2011-0030013) is also acknowledged.

References

[1] Choi, Y.-M., Malenica, Š., Clément, A., Bouscasse, B., and Ferrant, P. (2019). Poincaré's velocity representation in time domain free surface flow. In *IWWWFB2019, Newcastle, Australia*.

[2] Ferrant, P., Gentaz, L., Alessandrini, B., and Le Touzé, D. (2003). A potential/RANSE approach for regular water wave diffraction about 2-D structures. *Ship Technology Research*, 50(4):165–171.

[3] Hong, S., Kim, J., Cho, S., Choi, Y., and Kim, Y. (2005). Numerical and experimental study on hydrodynamic interaction of side-by-side moored multiple vessels. *Ocean Engineering*, 32(7):783 – 801. Deepwater Mooring Systems; Design, Analysis and Materials.

[4] Li, Z. (2018). *Two-phase spectral wave explicit Navier-Stokes equations method for wave-structure interactions*. PhD thesis, École Centrale de Nantes.

[5] Liang, H. and Chen, X.-B. (2017). A new multi-domain method based on an analytical control surface for linear and second-order mean drift wave loads on floating bodies. *Journal of Computational Physics*, 347:506 – 532.

[6] Malenica, Š. (1994). *Diffraction de troisième ordre et interaction houle-courant pour un cylindre vertical en profondeur finie*. PhD thesis, Universite Paris VI.

[7] Noblesse, F. (2001). Velocity representation of free-surface flows and Fourier-Kochin representation of waves. *Applied Ocean Research*, 23(1):41–52.

[8] Seng, S. (2012). *Slamming and whipping analysis of ships*. PhD thesis, Technical University of Denmark (DTU), Lyngby.

[9] Vukčević, V. (2016). *Numerical modelling of coupled potential and viscous flow for marine applications*. PhD thesis, University of Zagreb.